HEAT TRANSFER ON HLM COOLED WIRE-SPACED FUEL PIN BUNDLE SIMULATOR IN THE NACIE-UP FACILITY

Ivan Di Piazza[a*], Morena Angelucci[b], Ranieri Marinari[b], Mariano Tarantino[a], Nicola Forgione[b]

[a] Italian National Agency for New Technologies, Energy and Sustainable Economic Development, C.R. ENEA Brasimone, Italy.

[b] University of Pisa, Dipartimento di Ingegneria Civile e Industriale, Italy

* Corresponding author. E-mail: ivan.dipiazza@enea.it

ABSTRACT

The NACIE-UP experimental facility at the ENEA Brasimone Research Centre (Italy) allowed to evaluate the heat transfer coefficient of a wire-spaced fuel bundle cooled by lead-bismuth eutectic (LBE). Lead or lead-bismuth eutectic are very attractive as coolants for the GEN-IV fast reactors due to the good thermo-physical properties and the capability to fulfil the GEN-IV goals. Nevertheless, few experimental data on heat transfer with heavy liquid metals (HLM) are available in literature. Furthermore, just a few data can be identified on the specific topic of wire-spaced fuel bundle cooled by HLM. Additional analysis on thermo-fluid dynamic behaviour of the HLM inside the sub-channels of a rod bundle is necessary to support the design and safety assessment of GEN. IV/ADS reactors.

In this context, a wire-spaced 19-pin fuel bundle was installed inside the NACIE-UP facility. The pin bundle is equipped with 67 thermocouples to monitor temperatures and analyse the heat transfer behaviour in different sub-channels and axial positions.

The experimental campaign was part of the SEARCH FP7 EU project to support the development of the MYRRHA irradiation facility (SCK-CEN). Natural and mixed circulation flow regimes were investigated, with sub-channel Reynolds number in the range $\mathrm{Re} = 10^3 - 10^4$ and heat flux in the range $q" = 50 - 500 \left[kW/m^2 \right]$.

Local Nusselt numbers were calculated for five sub-channels in different ranks at three axial positions. Section-averaged Nusselt number was also defined and calculated. Local Nusselt data showed good consistency with some of the correlation existing in literature for heat transfer in liquid metals for rod bundles. Local Nusselt numbers in peripheral ranks are lower, due to the presence of the hexagonal external wrap which affects the temperature profile.

The good accuracy of the instrumentation and the error analysis implemented in the post-processing routines guaranteed a good reliability of the results. The data set presented can be used also to validate computer codes for HLM-cooled rod bundles.

LBE, 19-pin bundle, wire-spacer, heat transfer, natural circulation

INTRODUCTION

Among the reactor technologies being considered by the Generation IV International Forum (GIF), the heavy liquid metal-cooled systems seem to be a promising choice for the fulfilment of the Generation IV goals (GEN IV International Forum, 2014). Adequate physical and thermal properties of the heavy liquid metals (HLMs) increased the interest for their employment as coolant for nuclear systems. Nevertheless, due to the higher density and conductivity of lead and lead-bismuth eutectic (LBE) with respect to water, more detailed

analyses on the thermo-fluid dynamic behaviour of the HLMs are needed to support the development of innovative nuclear systems. For instance, liquid metals are characterized by a Prandtl number lower than unity, therefore the heat transfer mechanisms are strongly affected by the molecular thermal conduction, even at large Reynolds numbers. As a consequence, careful investigations are necessary for the evaluation of the heat transfer coefficient inside the sub-channels of a fuel rod bundle. This topic is a key aspect for the assessment of the coolability of the core during normal and accidental conditions.

Wire-spaced bundles were widely investigated due to their dominant application in the sodium technology, lot of works were accomplished from the '60s to '80s, when the interest for sodium technology was high. Lafay et al. (1975) and Bartholet et al. (1977 a) investigated the hydraulic behaviour of a wire wrapped rod bundle and measured the pressure field inside the sub-channels. Among the first experimental data on heat transfer in a rod bundle with wire-wrap spacers, some noticeable works appeared in the literature, e.g. the works of Fontana et al. (1973) and Wantland et al. (1976), which employed liquid sodium as coolant. A comprehensive state of the art regarding in-core thermal hydraulics US research activities during '60s and '70s was carried out by Kahn (1980). A summary of the Russian experience with the liquid metal-cooled fast reactor (LMFR) technology can be found in the IAEA technical document (IAEA, 1999). During the '50s and '60s, pioneering experience with experimental SFRs was acquired in USA (Fermi, EBR-I and EBR-II), France (Rapsodie) and Russia (BR-5/10 and BOR-60). It formed the basis for the commissioning and the operation prototype and full scale reactors, such as Phénix and Super Phénix (France), BN-350 (Kazakhstan), BN-600 (Russia), Monju (Japan), which have gained more than 100 reactor-years of experience (Aoto et al., 2014).

During the last years, the interest in the liquid metal technology increased again, due to the GEN. IV commitment and objectives: non-proliferation, economics, reduction of the long-life waste, safety, and more efficient use of the fuel. Even if the sodium-cooled fast neutron reactor technology is still considered the reference solution (e.g. ASTRID project, Le Coz et al., 2011), the lead-cooled fast reactor (LFR) seems to be a promising alternative technology for fast reactors. The LFRs features include a fast neutron spectrum with low absorption, high temperature operation, and being cooled by molten lead or lead-bismuth eutectic (LBE), low-pressure, chemically inert liquids with very good thermodynamic properties. The LFRs could use a closed fuel cycle enhanced by the fertile conversion of uranium. It can also be used as a burner to consume actinides from spent LWR fuel and as a burner/breeder with thorium matrices. An overview of the lead-cooled fast reactor activities is reported in Alemberti et al. (2014).

In this frame, several studies on thermal-hydraulic behaviour of HLMs were restarted too. Recently, an extensive review of the heat transfer correlations for heavy liquid metals was made by Pfrang and Struwe (2007). Their work reports proposed correlations for flow in a pipe, in triangular and square rod bundles. Mikityuk (2009) proposed a new correlation for rod bundles, based on four sets of experimental data available in literature. The correlation is compared with other existing correlations and an error analysis is also carried out. More recently, few works were focused on heat transfer in a fuel rod bundle cooled by heavy liquid metals. Pacio et al. (2014) investigated experimentally the heat transfer and pressure drop in a 19-rod bundle with grid spacer cooled by LBE. They found that measured Nusselt numbers are underestimated by the correlations existing in literature. Martelli et al. (2015) and Tarantino et al. (2015) measured for the first time the heat transfer coefficient for a 37-pin rod bundle with grid spacer cooled in a heavy liquid metal pool in the CIRCE facility (Turroni et al., 2001).They calculated the Nusselt number as a function of the Péclet number in forced and natural circulation flow, for Péclet numbers in the range 500-3000. The experimental data are slightly overestimated by the correlations used for comparison.

The present work studies the heat transfer with a heavy liquid metal in a wire-spaced fuel pin bundle simulator (FPS). For this purpose, a 19-pin fuel bundle was installed inside the NACIE-UP facility at the ENEA Brasimone R.C.. The facility was designed to operate in natural and gas-lift enhanced circulation regimes (Di Piazza et al., 2013). The FPS installed in the NACIE-UP facility was designed to be representative of the fuel assembly of the MYRRHA nuclear facility to be built at SCK-CEN (Abderrahim et al., 2001). The availability of local and overall experimental data in the FPS mock-up is of fundamental

interest for the design of the MYRRHA reactor. In this framework, the NACIE-UP experiment is focused on the low-intermediate mass flow rate and on the assessment of the coolability of the FA in these conditions. A similar experiment was carried out at KIT, but focused on the higher nominal mass flow rates (Pacio et al., 2015).The two experiments were carried out both in the context of the EU FP7 SEARCH project and are complementary.
The availability of experimental data is also a benefit for the validation of codes. In particular, turbulence and heat transfer models need to be extensively qualified for the applications to liquid metals, which are characterized by low Prandtl number. The validation of CFD and SYS-TH general purpose codes for HLM is a very important issue not only for design but also for safety analysis. In the H2020 European platform, some other projects are investigating in this direction (e.g. the SESAME project). Moreover, international benchmarks on the thermo-fluid dynamics of HLM-cooled FA are currently carried out. For example, the INERI-HiFifa benchmark is modelled on the 19-pin geometry of the NACIE-UP bundle and involves comparison between LES and RANS results (Doolaard et al., 2015).
In this work, the Péclet number range investigated is about 50-350. The test section was instrumented with 67 thermocouples (TCs), placed at three axial positions, which monitor wall and sub-channel temperatures allowing to calculate local and section-averaged Nusselt numbers. The collected data were post-processed by a Matlab routine. A comprehensive analysis on the heat transfer phenomena inside the FPS is reported in this study. It is mainly achieved by plotting Nusselt number as function of the Péclet number; this representation allowed the comparison of the experimental data with the correlations existing in literature.
In this paper, a detailed description of the experimental facility and of the test section is reported in Section 0. The post-processing method to analyse the collected data is described in Section 0. Section 0 discusses the main results on heat transfer obtained from the experimental tests. Finally, the main conclusions are given in Section 0.

EXPERIMENTAL SETUP

NACIE-UP facility

NACIE-UP is a rectangular loop consisting of two vertical pipes (O.D. 2.5") 8 meters long, working as riser and downcomer, connected by two horizontal pipes (O.D. 2.5") about 2.4 meter long, see the layout of the primary circuit in Figure 1. Pipes are made of stainless steel (AISI 304) and the total LBE inventory of the facility is about 200 l. In the bottom of the riser a prototypical wire-spaced fuel pin bundle simulator (FPS), with a maximum power of 235 *kW*, was installed. A heat exchanger (HX) is placed in the upper part of the downcomer. The difference in height between the centre of the heating section and the centre of the heat exchanger *H* is about 5.5 *m* and is essential for the onset of the natural circulation regime inside the loop. Furthermore, an argon gas injection device is placed inside the riser and, once operating, provides the driving force to sustain forced convection in the loop. An expansion tank is located at the end of the riser and it is partially filled with Argon as cover gas to avoid oxidation and to accommodate the thermal expansion of the LBE. An isolation 2.5" ball valve (V142), placed downstream of the FPS, can be partially closed to regulate the mass flow rate through the loop.

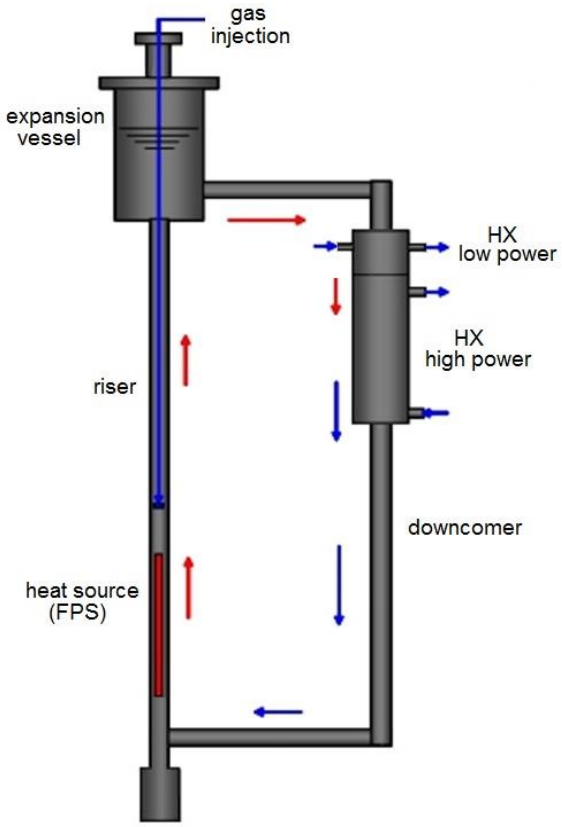

Figure 1: Schematic layout of the NACIE-UP facility primary loop.

The facility includes a secondary system, filled with water at 16 *bar*, connected to the HX, shell side. It is composed by a pump, a pre-heater, an air-cooler, by-pass and isolation valves, and a pressurizer with argon cover gas.
Then, an ancillary gas system ensures a proper cover gas in the expansion tank, provides the gas-lift injection in the riser, and allows the fill and drain system operation. This latter system is composed by ½" pipes, isolation valves and a storage tank.

The fuel pin bundle simulator (FPS)

The main component of the primary loop is the instrumented fuel pin bundle simulator, shown in Figure 2. It consists of 19 electrically heated pins with an active length L_{active} = 600 *mm*. The whole length (L_{tot} = 2000 *mm*) includes the non-active length and the electrical connectors. The lower non-active region of the bundle is more than 500 *mm* long, in order to have a fully developed flow at the inlet of the active zone. The pins have a diameter D=6.55 *mm* and are placed on a hexagonal lattice. Spacer grids are avoided thanks to the wire spacer. The maximum power of the fuel pin bundle is about 235 *kW*, corresponding to a maximum wall heat flux of 1 MW/m^2. A sketch of the cross section of the bundle is in Figure 3. The main dimensions are reported in Table 1.

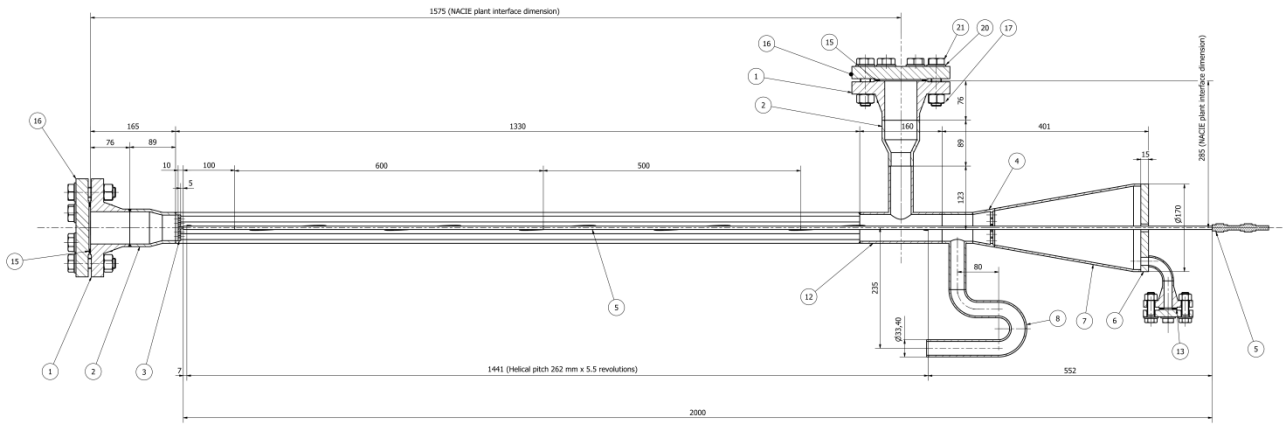

Figure 2: Overall bundle layout: technical drawing and picture.

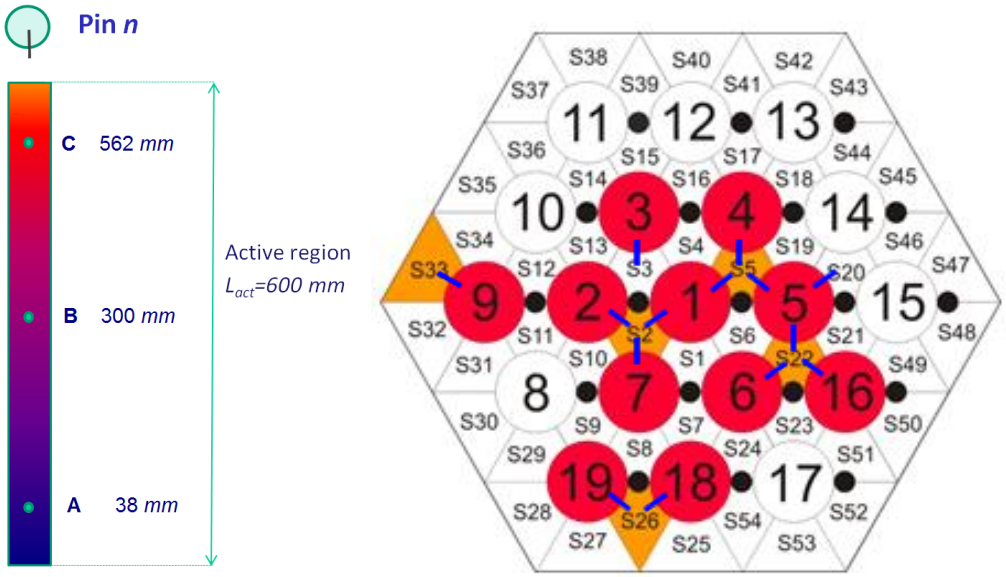

Figure 3: Axial position (left) and sketch of the monitored sections (right) of the fuel pin bundle simulator. Instrumented pins in red; instrumented sub-channels in orange, wires in black and wall TCs position in blue.

Table 1: Fuel pin simulator (FPS) main dimensions.

Dimension	Symbol	Value
Number of pins	M	19
Pin outer diameter	D	6.55 *mm*
Pitch	P	8.4 *mm*
Pitch-to-diameter ratio	P/D	1.2824
Wire diameter	d	1.75 *mm*
Wire pitch	P_w	262 *mm*
Total length	L_{tot}	2000 *mm*
Active length	L_{active}	600 *mm*
Total flow area	A	65.49 mm^2
Hydraulic diameter of the bundle	$D_{H,bdl}$	4.147 *mm*
Hydraulic diameter of the equivalent infinite lattice	$D_{H,nom}$	3.836 *mm*
Hexagonal wrapper apothem	a	19.67 *mm*

The total flow area can be conventionally divided into 54 sub-channels of three different ranks (S1-S54). The central rank is represented by the central pin 1 and by sub-channels S1-S6; the rank N-1 is represented by pins 2-7 and by sub-channels S7-S24; the external rank N is represented by the pins 8-19 and by sub-channels S25-S54. Three ranks are actually representative of the inner channel of a typical LFR fuel assembly. From detailed numerical comparative studies presented in literature (Gajapathy et al., 2009), it is known that, for wire-wrapped bundles of similar geometry, the influence of the wall is considered important for the external rank N and for the N-1 rank of pins, while the inner ranks are not so much affected by the hexagonal wrapper. The hydraulic diameter of an equivalent infinite lattice of rods, $D_{H,nom}$, is used to define the non-dimensional quantities in the post-processing of the results. This reference diameter was fixed in the context of the SEARCH project in agreement with the MYRRHA SCK-CEN design team (Van Tichelen, 2015).

Instrumentation

The instrumented sub-channels are illustrated in Figure 3. Instrumented pins are depicted in red and the monitored sub-channels are in orange. Three different axial positions are considered: z= 38, 300, and 562 *mm* after the beginning of the active region. Hereafter, it will referred to these sections as *A*, *B* and *C*. It should be mentioned that the three axial positions are exactly in the same configuration, being the wire pitch P_w=262 *mm*= 300-38 *mm*= 562-300 *mm*. This choice allows having three measurements of heat transfer referred to the same relative position of wire and pins. Pins 2, 4, 6, 7, 9, 16, 18, 19 are equipped with wall embedded thermocouples (0.35 *mm* thick) on a generatrix parallel to the pin axis. Pin 1 is instrumented with wall embedded thermocouples on two generatrices located 180° each other, parallel to the pin axis; pin 5 is instrumented along three generatices located at 120° each other. Pin number 3 is instrumented along a generatrix with 13 wall embedded thermocouples along the active length, placed every P_w/6=43.66 *mm* starting from z=38 *mm*. The total number of wall embedded thermocouples is 52. At each measurement section, wall embedded TCs move azimuthally around the pin to reach the correct azimuthal position, which is shown in **Figure 3**. The wall TCs are placed inside the clad, in a groove 0.38 mm thick. It is considered that the thermocouple measures the temperature at the junction (located at the centre) so a correction is needed to evaluate the temperature at the clad outer surface (see Section 0). Further, sub-channels S2, S5, S22, S26, S33 are instrumented with bulk thermocouples 0.5 *mm* thick, at the same three measurement sections z=38, 300, 562 *mm*, for a total number of 15 bulk thermocouples. The bulk thermocouples run following the wire associated to the pin closest to the monitored sub-channel (e.g. pin 1 for sub-channel S5). The hot junction is placed in the centre of the monitored sub-channel and the TC wire is prolonged to form an arc to increase its mechanical stiffness, aiming to guarantee the correct position when exposed to the LBE stream. The TC head is fixed to the spacing wire by point welding. All the thermocouples adopted in the FPS are 'K' type pre-calibrated by the manufacturer (THERMOCOAX) with a certified accuracy of 0.1 *K*.

In addition, the primary loop of NACIE-UP is equipped with 5 bubble tubes to measure LBE pressure inside the loop and other pressure transducers to monitor cover gas pressure. Then, several bulk thermocouples

monitor the temperature along the flow path in the loop. The mass flow rate is computed through the thermal balance.

Data acquisition and control system (DACS)

Data acquisition and instrumental control of both the primary and the secondary sides of NACIE-UP can be achieved remotely. The operations of fill and drain of the facility can be made remotely as well. The ancillary gas system, instead, is directly controlled through a gas panel placed near the facility. The number of pins activated and power ramp can be regulated as needed. Each pin can be controlled separately and this feature gives the opportunity to perform asymmetric heating tests in the future. However, in this work, only test with uniform heating of the FPS were performed.

Data acquisition starts once the temperatures inside the primary circuit are well established in a steady state condition. The frequency of the acquisition is 1 *Hz*. Each test lasts about 15-20 minutes in statistically stationary condition, in order to collect a significant set of data with a low error (about 1200 samples each test).

Experimental Test Matrix

The aim of the experimental campaign is to obtain stationary conditions in the facility and to characterize the local and overall heat transfer in the bundle. The test matrix included different power levels. For each power level, different mass flow rates were investigated, by changing the gas flow rate and/or by partial closure of the ball valve V142. As a first approximation, inlet temperature was not regarded, since the thermal-fluid dynamic behaviour of the bundle is largely independent of T_{in}. The reference quantities for each test are: the average velocity *u [m/s]*, which characterize the flow from a hydraulic point of view, and the average linear power in a single pin Q_{lin} *[kW/m]*, which defines the heat transfer boundary conditions. The range for the main parameters achievable with the NACIE-UP facility and considered in the experimental test matrix is reported in Table 2. The experimental test matrix with all the cases performed is reported in

Table **3**. Reynolds and Péclet numbers in

Table **3** are computed from the average temperature between temperatures at the inlet and at the outlet of the active region.

Table 2: Range of parameters achievable with NACIE-UP facility in Natural Circulation (NC) and Forced Circulation (FC) flow regime.

FLOW REGIME	$u\,[m/s]$	$\dot{m}\,[kg/s]$	Re	$\Delta T\,[°C]$	$Q\,[kW]$	$Q_{lin}\,[kW/m]$
NC	0.05 – 0.24	0.4 – 1.6	1200-5500	70-205	10-35	0.9 – 2.9
FC	0.10 – 0.59	0.7 – 4.0	2000-15000	30 - 190	20 - 110	1.9 – 9.5

Table 3: Experimental tests performed.

TEST NAME	$Q\,[kW]$	$\dot{m}\,[kg/s]$	$u\,[m/s]$	$\mathrm{Re}\cdot 10^{-3}$	Pe
P11X0	**11**	**1.06**	0.15	2.72	84
P102	**11**	**0.72**	0.10	1.93	55
103	**11**	**0.36**	0.05	1.13	26
P20X0	**20**	**1.49**	0.22	4.01	116
P204	**20**	**0.73**	0.11	2.24	52
P28X0	**28**	**1.17**	0.17	3.69	83
P212	**36**	**3.33**	0.49	10.06	242
P213	**36**	**2.22**	0.33	6.88	159
P214	**36**	**1.15**	0.17	3.96	77
P217	**43**	**3.2**	0.47	9.98	228

P218	**43**	**2.8**	0.41	8.75	199
P43X0	**43**	**1.62**	0.24	5.35	111
P223	**52**	**3.40**	0.50	10.81	237
P224	**52**	**2.24**	0.33	7.44	151
P265	**54**	**3.23**	0.47	10.21	226
P269	**108**	**3.95**	0.59	14.15	256

POST-PROCESSING METHODS

Definitions and derived quantities

For each monitored section, the bulk temperature is estimated from the measured sub-channel temperatures. Bulk TCs are positioned in the bundle sections in order to monitor the different kind of sub-channels (see Section 2.2). Since TCs are not homogeneously distributed inside the section, a weight averaged temperature is computed, as defined in Eq.(1). The 5 bulk thermocouples placed in each monitored section are multiplied by weighting factors. Weighting factors were chosen considering the fraction of the total flow area represented by the different instrumented sub-channels (S2, S5, S22, S26, S33), and are reported in **Table 4**. Weights w_2 and w_5 are equal and such that their sum is representative of the flow area of the central rank. w_{22} accounts for the total flow area of the second rank. The sum of w_{26} and w_{33} represents the flow area of the external rank.

A section-averaged wall temperature was defined in a similar way in Eq. (2). The wall temperature for each sub-channel, (e.g., $T_{w\,S2}$ for sub-channel S2) is the arithmetic average among the wall temperature related to that sub-channel (e.g. $T_{w\,S2} = \left(T_{w1} + T_{w2} + T_{w7}\right)/3$).

$$\overline{T}_b = T_{b\,S2}\cdot w_2 + T_{b\,S5}\cdot w_5 + T_{b\,S22}\cdot w_{22} + T_{b\,S26}\cdot w_{26} + T_{b\,S33}\cdot w_{33} \quad (1)$$

$$\overline{T}_w = T_{w\,S2}\cdot w_2 + T_{w\,S5}\cdot w_5 + T_{w\,S22}\cdot w_{22} + T_{w\,S26}\cdot w_{26} + T_{w\,S33}\cdot w_{33} \quad (2)$$

Table 4: Weights used to compute section-averaged temperatures.

w_2	w_5	w_{22}	w_{26}	w_{33}
0.058	0.058	0.346	0.179	0.359

The temperatures at the inlet and at the outlet of the heated region of the FPS (T_{in} and T_{out}) were obtained by linear extrapolation of the LBE bulk temperature measured in section A (38 *mm* after the beginning of the active zone) and section C (38 *mm* before the end of the active zone). It must be stressed that sections A and C are very close respectively to the inlet and outlet section of the active region of the FPS, which is 600 *mm* long. Figure 4 illustrates the values of the section-averaged bulk temperatures at the three sections and the extrapolated values across the heated length for a typical case. The bulk temperature at section B is practically coincident with the linear trend between sections A and C. This agreement justifies the linear assumption and the method chosen to find out T_{in} and T_{out}. Further, all the values of the T_{out} were compared with the LBE temperature measured by thermocouple TP102, located downstream the FPS, outside the test section. The difference between the two temperatures never exceeds 5°C. Moreover, the relative error on the temperature difference across the FPS considering T_{out} or TP102 as the outlet temperature is on average less than 1.7%. The good agreement provides arguments for the linear extrapolation method to obtain the temperature across the bundle. Moreover, it validates the use of the weighted average definition for bulk and wall temperatures in the overall section.

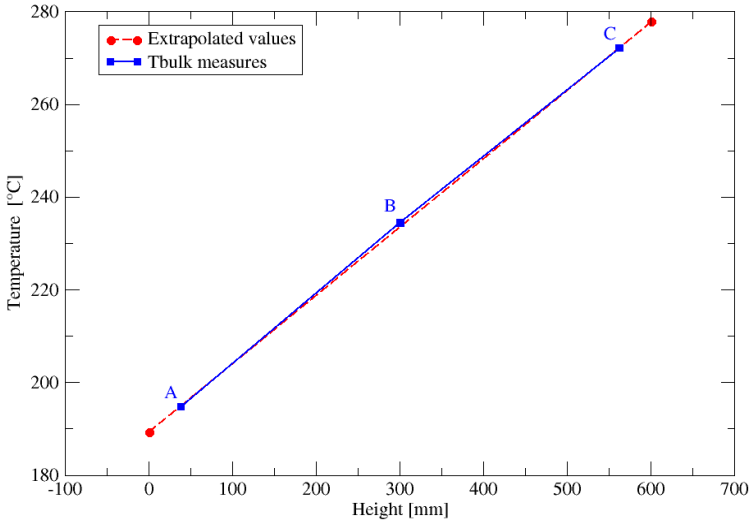

Figure 4: LBE average bulk temperature measured at three reference sections and extrapolated values for T_{in} and T_{out}.

As mentioned in Section 0 wall temperatures are measured by embedded thermocouples 0.35 *mm* thick, placed inside the clad, in a groove 0.38 *mm* deep. This kind of thermocouple mounting system does not modify the geometry of the pin, which remains cylindrical and the fluid flow and heat transfer in the sub-channel are not perturbed. However, wall embedded TCs measure a temperature in a position slightly inside the clad, higher than at the clad outer surface. A correction for this effect is implemented by applying the heat conduction law in cylindrical geometry, see Eq. (3).

$$T_w = T_{ac} - \frac{Q}{2\pi M L_{active}\, k_{ss}} \ln\left(\frac{D/2}{D/2-\delta_g}\right) \tag{3}$$

T_{ac} is the acquired TC temperature, M is the number of pins in the bundle, k_{ss} is the conductivity of stainless steel at T_{ac}. Q is the power released within the active length L_{active} and is 97% of the total power released. In fact, about 3% of the nominal power is released outside the active region due to losses in the cold tails and in the non-active part. This efficiency factor was provided by Thermocoax (LeCharpentier, 2015) and it is a construction feature. Then, δ_g is the distance between the centre of the TC and the cladding outer surface. The uncertainty in the radial position of the TC junction with respect the outer surface of the clad (maximum 0.015 *mm*) is considered in evaluating the wall temperature uncertainty.
As the differences between bulk and wall temperatures in some cases are quite small, due to the good heat transfer properties of the LBE, this correction is necessary for a correct estimation of the Nusselt number. To have an idea of the importance of this correction, the Biot number (Bi) was calculated for the distance δ_g. Biot number for the extrapolation distance is defined in Eq. (4), where h is the heat transfer coefficient calculated through $\overline{T}_b$ and $\overline{T}_w$ as defined respectively in Eq. (1) and (2).

$$\mathrm{Bi}_{extr} = \frac{h \cdot \delta_g}{k_{ss}} \tag{4}$$

It represents the ratio between the thermal resistance in the thermocouple wall thickness and in the boundary layer of the fluid. On average, 22% of the temperature drop occurs inside the extrapolation distance ($\mathrm{Bi}_{extr} \approx 0.22$). If this temperature jump is not considered to occur inside the clad but is incorporated inside the convective heat transfer term, significant errors are made in the analysis of the heat transfer phenomena.

The mass flow rate is calculated through the thermal balance across the heated length of the test section. The mass flow rate is obtained through Eq. (5) where $\bar{c}_p$ is the LBE specific heat at average temperature between FPS inlet and outlet, while Q is the power released within the active length.

$$\dot{m} = \frac{Q}{\bar{c}_p (T_{out} - T_{in})} \tag{5}$$

In Figure 5, all the performed cases are reported. For cases at lower power, tests at pure natural circulation are performed (green circles). The cases on the left of the natural circulation curve (green line) are performed with valve V142 partially closed. For the remaining cases, the gas-lift system is active.

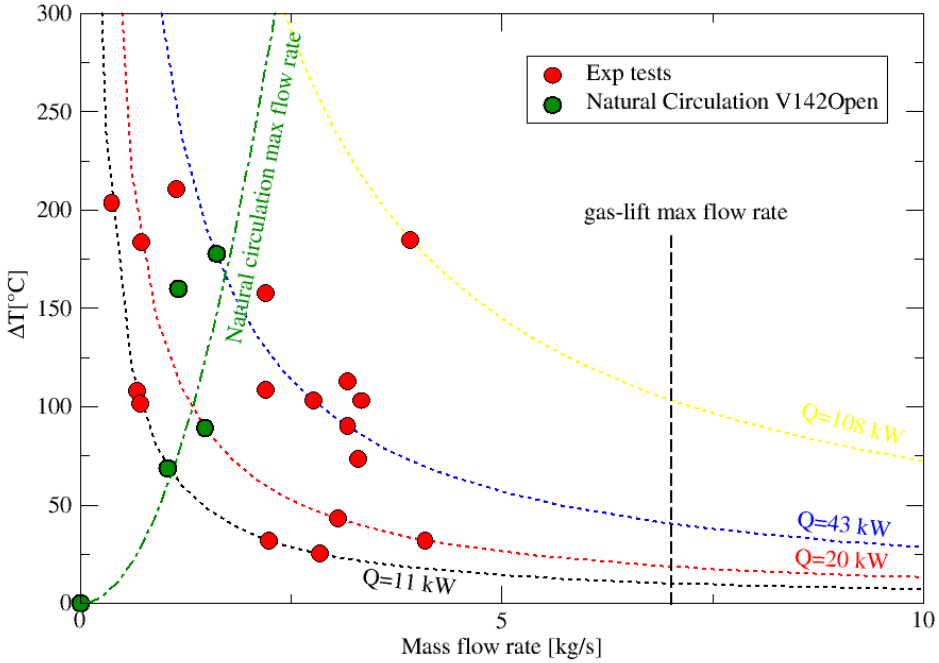

Figure 5: Temperature difference across the bundle against overall mass flow rate for all the test cases.

For post-processing analysis, some non-dimensional numbers were used. Reynolds number Re was calculated as in Eq. (6), Prandtl number is reported in Eq. (7) and Péclet number in Eq. (8).

$$\mathrm{Re} = \frac{\dot{m}\, D_{H,nom}}{A\, \mu} \tag{6}$$

$$\mathrm{Pr} = \frac{\mu\, c_p}{k} \tag{7}$$

$$\mathrm{Pe} = \mathrm{Re} \cdot \mathrm{Pr} \tag{8}$$

In this work, different definitions of the Nusselt number were employed. The local definition is reported in Eq. (9), where $T_{b,sc}$ is the temperature measured in the centre of the sub-channel and $T_{w,sc}$ is the average among the wall TCs of the related sub-channel. k is the LBE conductivity at the temperature $T_{b,sc}$. Then, an average Nusselt number (Nu_1) was defined as reported in Eq. (10). In this case, the section-averaged temperatures $\bar{T}_w$ and $\bar{T}_b$ are used to obtain the heat transfer coefficient h.

$$\mathrm{Nu_{sc}} = \frac{\mathrm{q"}}{\left(\mathrm{T_{w,sc}} - \mathrm{T_{b,sc}}\right)} \cdot \frac{\mathrm{D_{H,nom}}}{\mathrm{k}} \tag{9}$$

$$\mathrm{Nu_1} = \frac{q"}{\left(\overline{T}_w - \overline{T}_b\right)} \cdot \frac{D_{H,nom}}{k} \tag{10}$$

If not further specified, LBE properties in Eqs. from (6) to (10) are evaluated at temperature $\overline{T}_b$, according to formulas in Section 0.

LBE physical properties

In the present work, LBE physical properties, which are all temperature-dependent, are evaluated using empirical correlations suggested in the OECD/NEA Handbook (Nuclear Energy Agency, 2015). Formulas for density, specific heat, dynamic viscosity, conductivity are reported in Table 5. The maximum deviation of the experimental data with respect to the correlation is also reported. The standard deviation of the experimental data with respect to the related correlation was computed from the source data reported in the OECD/NEA Handbook (Nuclear Energy Agency, 2015) for each physical property and it is reported in the last column.

Table 5: Physical properties of LBE as a function of temperature (T in Kelvin), from LBE-Handbook (Nuclear Energy Agency, 2015).

Property	Symbol	Correlation	Maximum Uncertainty	Standard deviation
Density	$\rho(\mathrm{T})$	$11065 - 1.293 \cdot T$	$\leq 0.8\%$	0.58%
Heat capacity	$c_p(T)$	$164.8 - 3.94 \cdot 10^{-2} \cdot T + 1.25 \cdot 10^{-5} \cdot T^2 - 4.56 \cdot 10^{-5} \cdot T^{-2}$	$\leq 5.0\%$	2.4%
Dynamic viscosity	$\mu(\mathrm{T})$	$4.94 \cdot 10^{-4} \exp\left(\frac{754.1}{T}\right)$	$\leq 6.0\% - 8.0\%$	7.2%
Thermal conductivity	$k(T)$	$3.284 + 1.67 \cdot 10^{-2} \cdot T - 2.305 \cdot 10^{-6} T^2$	$\leq 10.0\% - 15.0\%$	6.2%

Uncertainty analysis

In this work, several sources of uncertainties need to be taken into account. For each raw measured quantity *X*, two sources of error must be considered, i.e. the sampling statistical error and intrinsic instrumental error. The total uncertainties for each acquired variable is computed as in Eq. (11).

$$\sigma^2_{Xi,tot} = \sigma^2_{Xi,stat} + \sigma^2_{Xi,instr} \tag{11}$$

Another source of error to be considered is the uncertainty on the LBE physical properties, and the value indicated in the last column of Table 5 are used for this purpose.

Following the error propagation theory , the uncertainties of a derived quantity Y ,which is function of n variables X_i (Eq. (12)), is computed from the standard deviation of the n variables, following Eq. (13).

$$Y = f\left(X_1, ..., X_n\right) \tag{12}$$

$$\sigma^2_Y = \sum_{i=1}^{n} \left(\frac{\partial f}{\partial Xi} \cdot \sigma_{Xi} \right)^2 \tag{13}$$

In Table 6, the results of the error analysis for the primary and derived quantities are presented. The statistical error on the primary variables are very low, with an average value below 1% and a maximum value of 2.7%. For the mass flow rate, the average error is 8.8% and the maximum is 15.1%. Statistical error on Re and Pe are larger than those on the mass flow rate and largely affected by the uncertainty on the physical

properties. The maximum error on the Peclet number is around 19%. Regarding the Nusselt number, the statistical error increases from section A to section C due to the increasing error of the wall-bulk temperature difference, with average and maximum values of 18% and 36% for section C. The average error on the overall Number is around 14%.

Table 6: Average and maximum standard deviation of the primary and derived quantities.

Variable	$\langle \sigma_X \rangle$	$\max(\sigma_X)$	$\left\langle \frac{\sigma_X}{X} \right\rangle$	$\max\left(\frac{\sigma_X}{X} \right)$
Primary variable				
Q	39.9 *W*	75.0 *W*	0.13%	0.40%
ΔT_{FPS} [°C]	1.3 °C	3.2°C	1.00%	2.70%
Secondary variables				
$\dot{m}$	0.19 *kg/s*	0.47 *kg/s*	8.8%	15.1%
$\overline{T}_{wA} - \overline{T}_{bA}$	0.42 °C	1.08 °C	6.10%	10.4%
$\overline{T}_{wB} - \overline{T}_{bB}$	0.95 °C	2.39 °C	13.1%	26.9%
$\overline{T}_{wC} - \overline{T}_{bC}$	1.20 °C	3.15 °C	16.4%	36.1%
non-dimensional variables				
Re_A	653	1450	11.5%	16.7%
Re_B	744	1570	11.5%	16.7%
Re_C	830	1700	11.5%	16.7%
Pe_A	24.4	48.1	15.2%	19.4%
Pe_B	22.8	46.2	15.2%	19.4%
Pe_C	21.3	44.2	15.2%	19.4%
Nu_{1A}	0.66	0.90	8.80%	12.1%
Nu_{1B}	0.91	0.95	14.1%	28.0%
Nu_{1C}	1.15	2.70	17.8%	36.6%
Nu_1	0.90	2.70	13.6%	36.6%

EXPERIMENTAL RESULTS

In this section, a comprehensive analysis on FPS behaviour and heat transfer coefficient is presented. This study is mainly achieved through the analysis of the Nusselt number, defined in Section 0. Nusselt number is plotted as a function of the Péclet number to allow a comparison with the correlations existing in literature. A literature review on fluid flow and heat transfer in wire-spaced bundles was presented in Section 0. Few works focus on the temperature distribution inside the bundle but none of them suggests a specific correlation to be used for wire-spaced geometry in liquid metals. For this reason, the correlations used for comparison were chosen among the ones mainly intended for bare rod bundles and obtained from a large number of experimental data. These correlations are the most used in the field of HLM technology.

- The first one, in Eq. (14), was suggested by Ushakov (1977) and it is valid for triangular and square lattice of rods in the range $1.3 \le P/D \le 2.0$ and $1 < Pe < 4000$.

$$Nu = 7.55\frac{P}{D} - 20\left(\frac{P}{D}\right)^{-13} + \frac{3.67}{90\cdot\left(\frac{P}{D}\right)^2}\cdot Pe^{\left(0.56+0.19\cdot\frac{P}{D}\right)} \quad (14)$$

- The second one, in Eq. (15), is the correlation by Mikityuk (2009), which was obtained from four independent sets of experimental data, mainly on triangular rod bundles. The validity range is $30 < \mathrm{Pe} < 5000$ and $1.1 \le P/D \le 1.95$.

$$\mathrm{Nu} = 0.047 \cdot \left(1 - e^{-3.8 \cdot \left(\frac{P}{D} - 1\right)}\right) \cdot \left(\mathrm{Pe}^{0.77} + 250\right) \tag{15}$$

- The third correlation is from Kazimi and Carelli (1976) and is reported in Eq. (16). It was obtained using several experimental campaigns with different liquid metals (Na, Hg and NaK) and it is recommended for the ranges $10 < \mathrm{Pe} < 5000$ and $1.1 \le P/D \le 1.4$.

$$\mathrm{Nu} = 4 + 0.16\left(\frac{P}{D}\right)^{5} + 0.33\left(\frac{P}{D}\right)^{3.8} \cdot \left(\frac{\mathrm{Pe}}{100}\right)^{0.86} \tag{16}$$

Results are presented in next two sections. At first, local analysis is discussed in Section 0. It regards the computation of the Nusselt number for the single sub-channels. Overall section-averaged heat transfer is discussed in Section 0.

Local heat transfer

The local Nusselt number, defined in Section 0 Eq. (9), allows evaluating the heat transfer capability for the single sub-channel. In particular, the sub-channels of the central rank are representative of the sub-channel of an infinite lattice, so their behaviour is of relevant interest.

Figure 7 and **Figure 7** show the results for sub-channels S2 and S5, the monitored points of the internal rank. Most plotted data set very close to the Ushakov and Mikityuk correlations. Some data in sub-channel S5 exhibit lower values closer to the Kazimi and Carelli correlation. The experimental points at section C of sub-channel S2 are not considered. For these data, the temperature differences between wall and bulk are very small, especially at very low mass flow rate, and the uncertainty is high. Moreover, it can be noticed that the Nusselt number in sub-channel S2 is generally higher than in S5.The differences between the two internal sub-channels S2 and S5 can be explained by considering the position of the wire with respect to the sub-channel, depicted in **Figure 3**. It should be mentioned that the wire's orientation is right-handed. So, for sub-channel S2 the wire of pin 2 passes through the considered sub-channel in an axial position a little upstream the monitored sections. Instead, the wire of pin 1 passes through sub-channel S6 before the monitored section, where then overlooks sub-channels S5. In previous works (Lafay et al. (1975), Kahn (1980)), the effect of the wire on the velocity field was investigated. Peripheral swirl flow in sub-channels containing the wire was observed, which also causes temperature asymmetries inside the bundle (Wantland et al. (1976)). The turbulent swirl flow, caused by the wire-spacer, can be the cause of the heat transfer enhancement, which also explains the high values of Nusselt number.

Figure 8 displays the local values of the Nusselt number for the sub-channel S22. The results give generally relatively high Nusselt numbers, which are in agreement with the Ushakov and Mikityuk correlations. Few data are quite above the correlations suggested by literature. Most of them belongs to section A in which thermal field is not yet developed. Even if sub-channel S22 belongs to rank *N-1*, between the internal and the external ones, the Nusselt numbers are quite in agreement with the results for the internal sub-channels, i.e. S2 and S5. In Bartholet et al. (1977 b), it was demonstrated that sub-channels belonging to rank *N-1* closer to the internal ones (e.g. S22) show a behaviour similar to these latter. On the other hand, sub-channels belonging to rank *N-1* closer to the side sub-channels (e.g. S21 and S23) are affected by the external wrapper.

In **Figure 9** and **Figure 10**, results for the sub-channels S26 (side) and S33 (corner), belonging to peripheral rank *N*, are shown. For these sub-channels the thermal field is affected by the presence of the hexagonal wrapper. In fact, the conjugate heat transfer to the outer structures plays a crucial role and moreover they are heated only from the inner side of the bundle. Therefore a different behaviour is expected with respect to the

central sub-channels (Rolfo et al., 2012). In particular, the temperature difference between the wall and the middle of the sub-channel increases and the Nusselt number decreases. The Nusselt number for sub-channel 26 is generally lower with respect to the internal ranks. The experimental points are even overestimated by the Carelli-Kazimi correlation, which is quite conservative. With respect to sub-channel S26, Nusselt numbers in S33 are higher and are generally in accordance with the Carelli-Kazimi correlation.

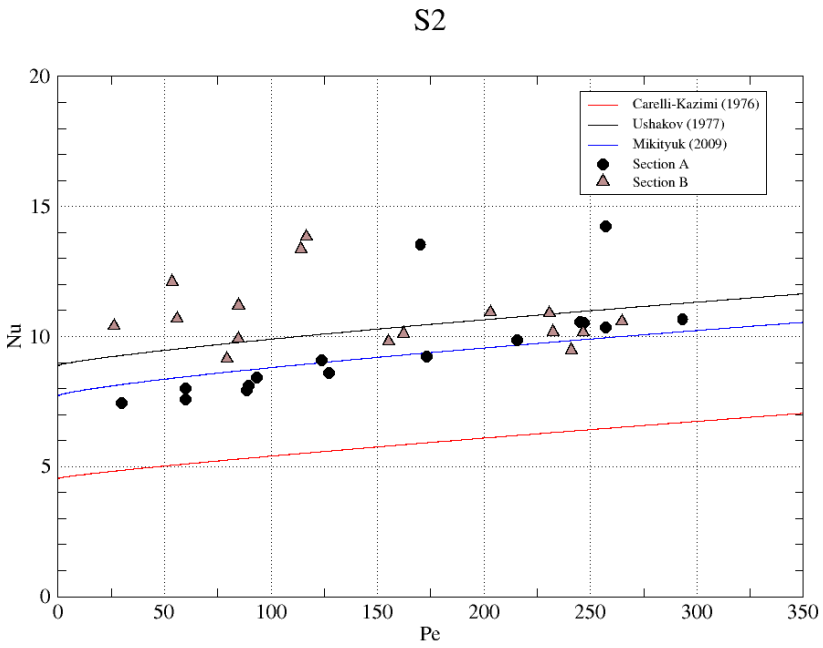

Figure 6: Experimental data of local Nusselt versus Péclet for the internal rank, sub-channel S2.

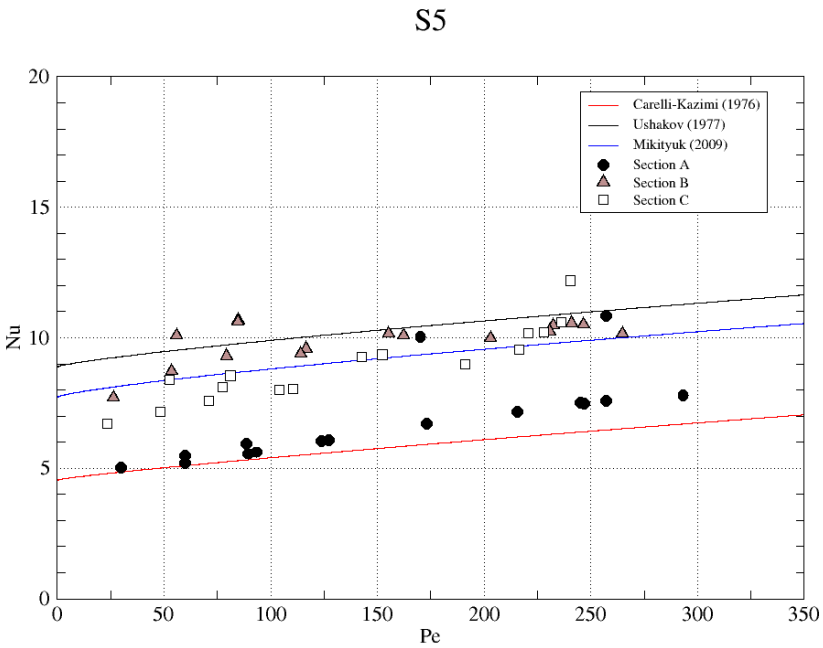

Figure 7: Experimental data of local Nusselt versus Péclet for the internal rank, sub-channel S5.

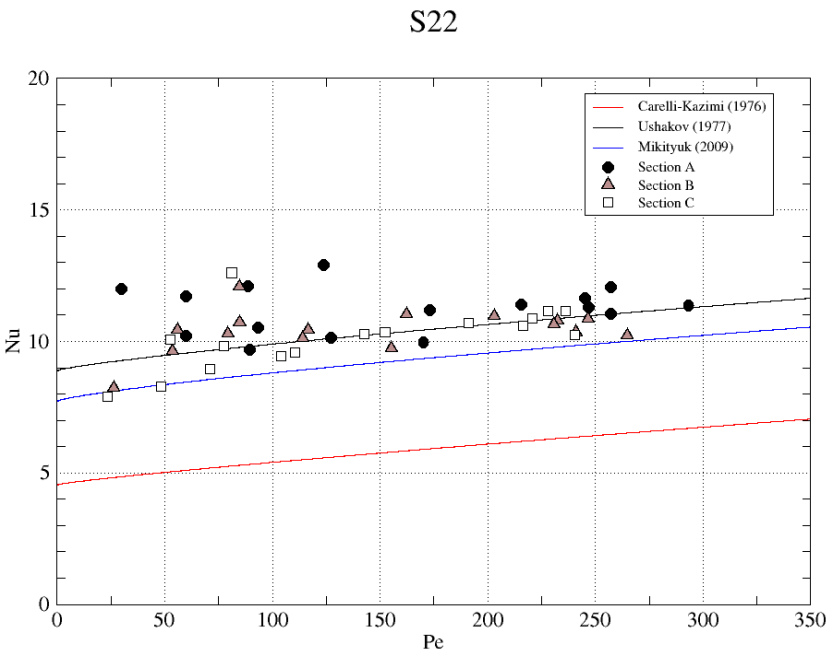

Figure 8: Experimental data of local Nusselt versus Péclet for the rank N-1, sub-channel S22.

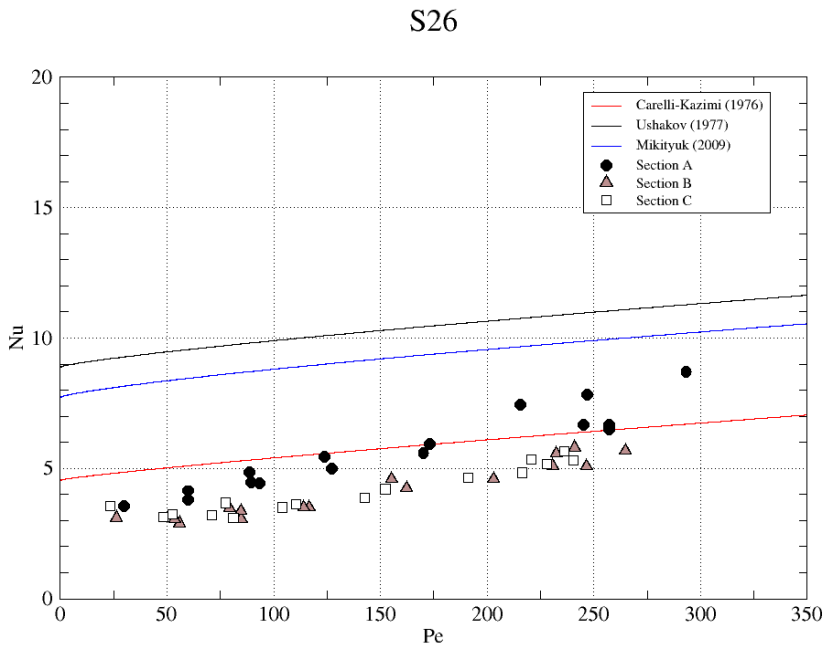

Figure 9: Experimental data of local Nusselt versus Péclet for the rank N, sub-channel S26.

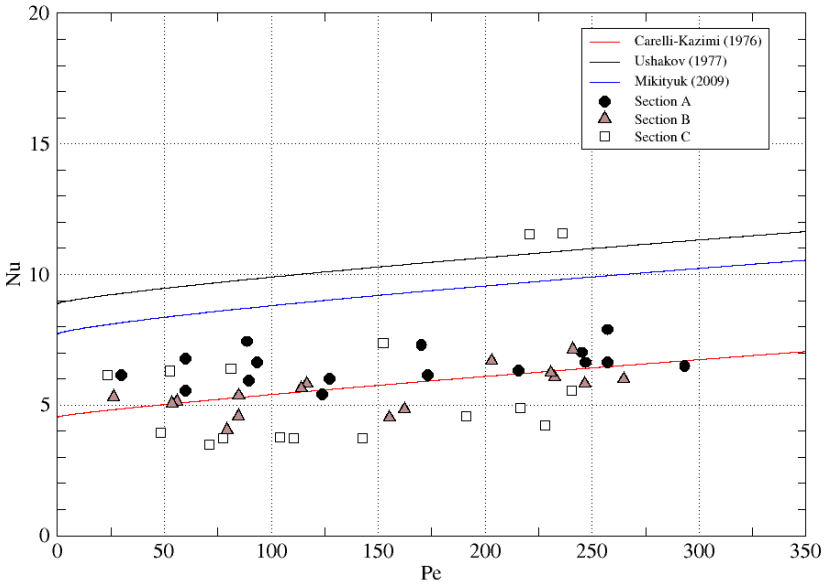

Figure 10: Experimental data of local Nusselt versus Péclet for the rank N, sub-channel S33.

Overall heat transfer

Experimental results for the section-averaged Nusselt number Nu_1, defined in Section 0 Eq. (10), are reported in Figure 11. Nu_1 is computed from the section-averaged wall and bulk temperature. The following values are generally quite low and almost all the data stay between the Carelli and the Mikityuk correlations. It is clear that this definition of Nusselt is widely affected by the colder LBE in the peripheral rank, which results in significant wall-bulk temperature differences. The general trend of the data is in agreement with the existing correlations with a similar slope with respect to the Péclet.

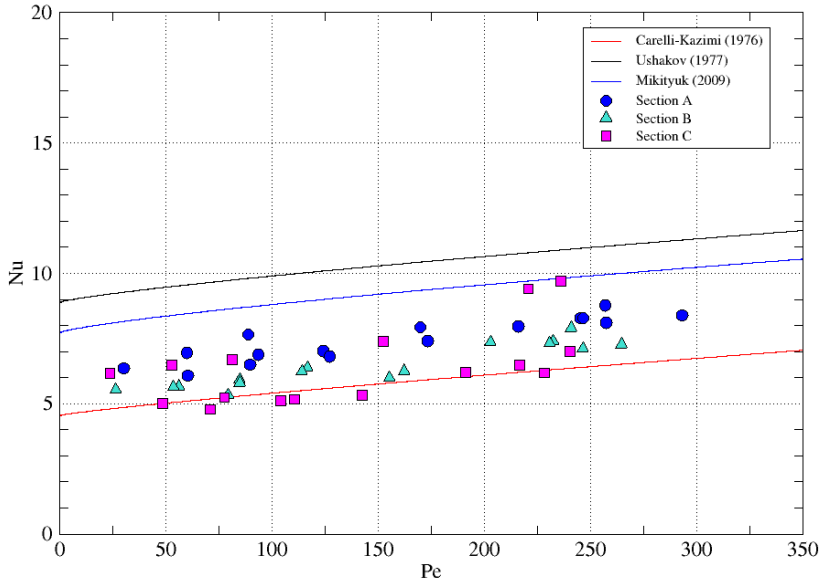

Figure 11: Section-averaged Nusselt number Nu_1 for all test cases at sections A, B, C.

Figure 12 shows the maximum clad temperature for each test performed in the NACIE-UP facility. The experimental data are reported as function of the mass flow rate and the power level. For a fixed value of the mass flow rate, the temperature difference across the bundle increases as the power level increases. The dotted line connects all the cases at same power level, e.g. 11 *kW*. This graph can help to identify the range of

operability of the facility for the low mass flow rate range. For a set power level, it is possible to estimate the lowest mass flow rate achievable without exceeding the temperature limits. Decreasing the power level, it will be possible to reach lower mass flow rate in safe conditions. It is possible to re-scale these results for the MYRRHA FA and therefore good indications on the operability of the MYRRHA facility can be deduced.

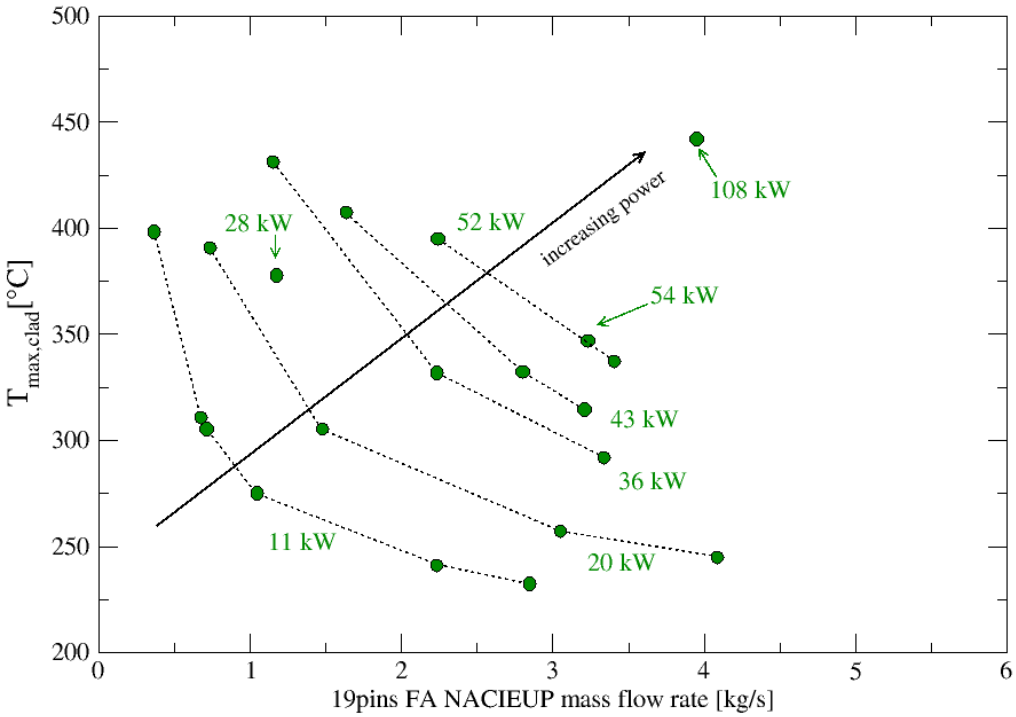

Figure 12: Maximum clad temperature achieved in the NACIE-UP facility for each test case.

Test cases P218 and P43X0

In this section, some details of two test cases are presented. Both tests are characterized by nominal power of 43 *kW*, but differ for the flow regime inside the loop. P43X0 is natural circulation flow, while for P218 a certain volume rate of argon gas is injected in the riser to enhance the circulation of LBE inside the loop. The main thermal-hydraulic parameters related to these tests are reported in Table 7.

Table 7: Main thermal hydraulic parameters of the cases P43X0 and P218.

	$Q[kW]$	Gas flow rate [*Nl/min*]	T_{in} [°C]	T_{out} [°C]	ΔT_{FPS} [°C]	$\dot{m}$ [*kg/s*]	u [*m/s*]
P43X0							
Average value	43	-	226.1	404.2	178.1	1.61	0.248
σ	0.05	-	0.4	0.7	0.77	0.09	0.014
P218							
Average value	43	5.0	240.0	343.1	103.1	2.76	0.408
σ	0.05	0.4	0.7	2.7	2.83	0.27	0.041

In Figure 13, the axial distributions of the weighted temperatures $\overline{T}_b$ and $\overline{T}_w$ are shown. In the same figures, the wall temperatures on pin 3, equipped with 13 TCs along the active region, are also reported. The wall and bulk temperatures seem to have quite parallel slope along the axial coordinate. However, the wall-bulk temperature difference tends to increase for higher axial position in both the cases. The difference is more noticeable considering the slope of pin 3 wall temperature with respect to the bulk temperature. The different slope of bulk temperature and wall average temperature is the evidence that the temperature field is not yet fully developed in the whole active region (L_{active} = 600 *mm*).

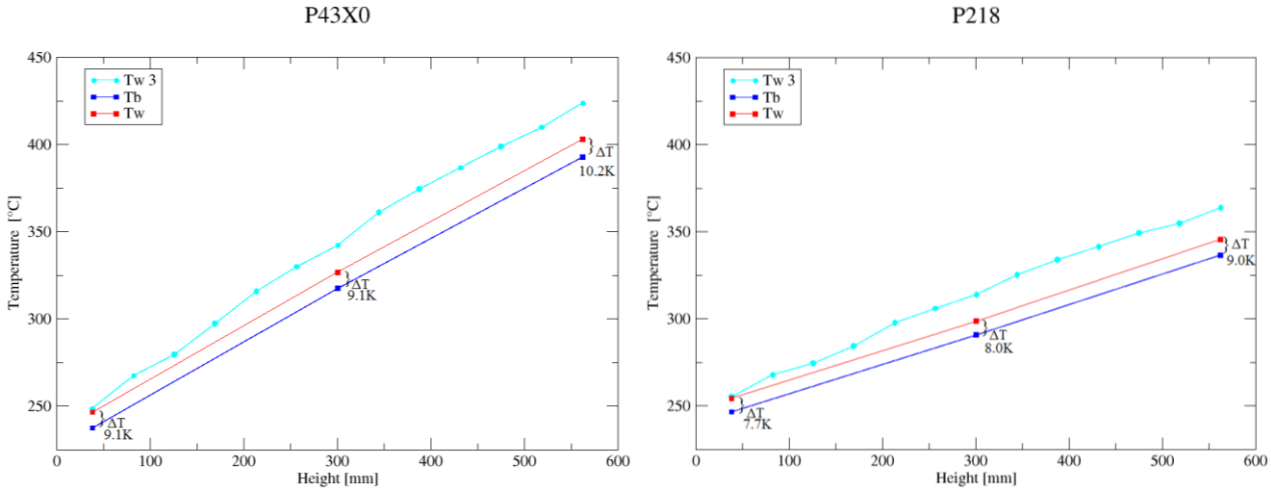

Figure 13: Axial distribution of average bulk and wall temperatures and pin 3 wall temperature, test P43X0 and P218.

In Figure 14, the time trend of local wall and bulk temperature for sub-channels S5 and test P43X0 is shown. Even if trends exhibit some oscillations, the same oscillations are similarly displayed in all the TCs of the sub-channel. Therefore, the difference between wall and bulk temperatures remains quite accurate, oscillating in a range of 0.5 °C. It means that TCs are capable of catching the local heat transfer coefficient quite accurately also when wall-bulk temperature differences are relatively small. For the case reported, this quantity is always more than 5°C. In some cases the wall-bulk temperature difference can decrease to 2-3 °C or below. It happens frequently for the sub-channel S2 in section C. In this case the Nusselt number is strongly affected by the TCs accuracy and the computed values are not reliable. These data are excluded from the data set and are not presented here.

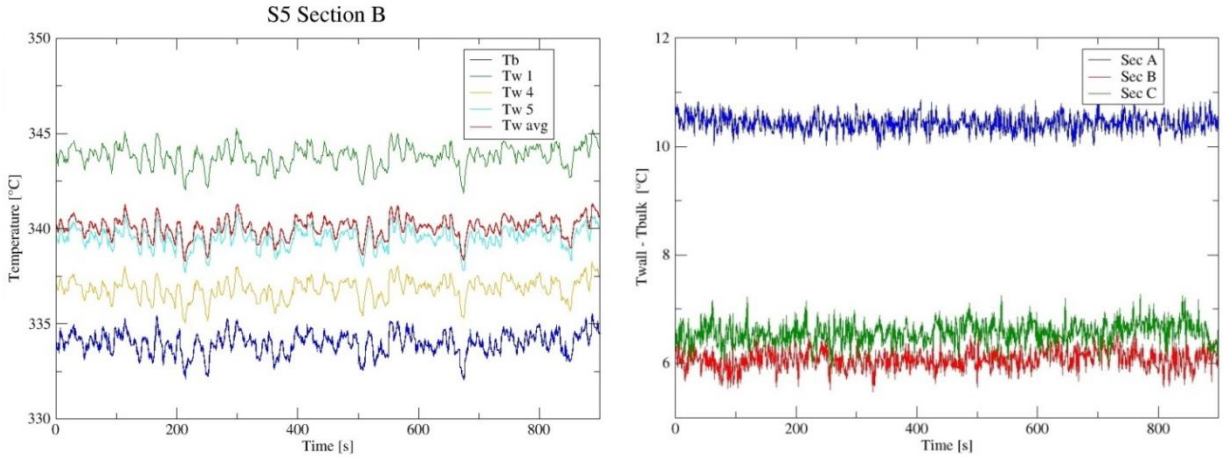

Figure 14: Time trend for wall, bulk temperatures and their differences in sub-channel S5 for case P43X0.

CONCLUSIONS

In this work, the NACIE-UP facility, located at ENEA Brasimone Research Centre, is described. A test section was designed and manufactured in order to perform experiments for thermal-hydraulic studies of a wire-spaced fuel pin bundle cooled by HLM. It consists of 19 electrical pins, placed in a hexagonal lattice by a suitable wrapper, while spacer grids will be avoided thanks to the wire spacer.

To the authors' knowledge, most of the data on heat transfer for wire-spaced bundle cooled by a liquid metal available in literature consider sodium as coolant. Few recent experimental studies focused on heat transfer phenomena in heavy liquid metal cooled fuel bundle test section with grid spacers instead of wire-spaced rods.

The experimental campaign performed at ENEA with the NACIE-UP facility was intended to investigate a range of low LBE mass flow rate, $\dot{m} \approx 0.3-4.0\ kg/s$, $Q_{lin} \approx 1-10\ kW/m$, $Q \approx 10-110\ kW$. The sub-channel Reynolds and Péclet numbers were respectively <12000 and <400, in the laminar or early transitional range. Tests with natural circulation and gas-lift enhanced circulation flow regimes were performed.

In this paper, details on the procedures of the experimental tests, on the post-processing methods are described. Data acquisition started after that statistical steady state conditions were reached and data collection lasted about 20 minutes (1200 samples) in order to have a set of data statistically relevant.

Measurements of wall thermocouples proved to be quite accurate. Some oscillations are presents in the signal, but the same oscillating trend is exhibited by all the TCs in the same sub-channel. Therefore, the wall-bulk temperature difference remains quite constant with an acceptable error. Temperature differences $T_w - T_b$ up to 2.5-3°C are detected with good accuracy. The data set selected showed an average relative error on the Nusselt number of 13%.

Then a comprehensive analysis on the heat transfer phenomena inside the FPS is presented. This study is mainly achieved through the analysis of the Nusselt number, graphically reported as a function of the Péclet number. This representation allows the comparison of the experimental data with the correlations existing in literature. Among them, three were chosen for comparison.

Two different analyses for heat transfer were performed: local analysis in single sub-channel and overall section analysis. Results on local analyses generally show consistency. Nusselt numbers in central channels are well represented by two of the correlation chosen. Nusselt in peripheral sub-channels are lower as the thermal field is affected by the heat transfer to the outer structures. This is a key feature of the HLM cooled bundle thermal-hydraulics, where temperature difference in a section can be high, up to 50 °C in nominal conditions, and there is a substantial difference between central channel temperature and section-average bulk temperature. For the overall section analysis, a section-averaged Nusselt number (Nu_I) was defined based on section-averaged temperatures. Results showed values between the Carelli-Kazimi and the Mikityuk correlations, and the slope of the experimental trend is very similar to the correlations. The data set selected showed an average relative error on the Nusselt number of 13%.

The comparison of the experimental data with correlations is a good practice to investigate the global coherence of the data set, but the specific geometry in the specific flow rate range with heavy liquid metals probably was never investigated from experimental point of view in the past. Moreover, correlations for complex geometries (like fuel pin bundles) are generally based on largely non-uniform experimental data sets. This non-uniformity is due to: the type of fluid employed (sodium, galistan, lead, etc..), the geometry investigated (wire vs. grid), the experimental setup conditions, the experimental measurement techniques, and the definitions adopted for the heat transfer coefficient and Nusselt number. From this remark, probably the best practice is simply to describe accurately the experimental setup and the definitions adopted and to be very careful in comparison with correlations or other experimental data sets.

Although relevant results were obtained, future developments are foreseen. The full range of power and mass flow rate needs to be investigated and the repeatability of the test verified. For this purpose, the equipment of the facility will be improved in instrumentation and operational conditions. Differential pressure transducers will be installed on the test section to perform accurate measurements of the pressure losses across the fuel pin bundle simulator and the pressure head provided by the gas injection system. An appropriate flow meter will be also installed to control the LBE mass flow rate during tests which simulate transient conditions.

Acknowledgements

The authors would like to acknowledge the support of the European Commission in the framework of the European FP7 SEARCH project grant number 295736.

Nomenclature

Roman letters

A	Flow area in the fuel pin bundle
a	Apothem of the hexagonal wrapper
Bi	Biot number
c_p	Specific heat capacity
D	Pin diameter
$D_{H,bdl}$	Hydraulic diameter of the 19-pins bundle
$D_{H,nom}$	Hydraulic diameter of infinite lattice equivalent bundle
d	Wire diameter
H	Difference in height between heat source and heat sink
h	Heat transfer coefficient
k	Conductivity
L	Length
M	Number of pins
$\dot{m}$	Mass flow rate
N	Number of pin rank
Nu	Nusselt number
P	Bundle pitch
P_w	Wire pitch
Pe	Péclet number
Pr	Prandtl number
Q	Bundle total power
Q_{lin}	Linear power
q''	Wall heat flux
Re	Reynolds number
T	Temperature
$\bar{T}$	Section-averaged Temperature
T_{ac}	Acquired Temperature
u	Average axial Velocity
z	Vertical coordinate from the beginning of the active region

Greek Letters

δ_g	Distance between the centre of wall TCs and the clad outer surface
ΔT	Temperature difference
μ	Dynamic viscosity
ρ	Fluid density
σ_X	Standard deviation of generic variable X

Abbreviations and acronyms

ADS	Accelerator-driven System
CFD	Computational Fluid Dynamics

DACS	Data Acquisition and Control System
EBR	Experimental Breeder Reactor
FA	Fuel Assembly
FC	Forced Circulation
FPS	Fuel Pin bundle Simulator
GIF	Generation IV International Forum
HX	Heat Exchanger
HLM	Heavy Liquid Metal
IAEA	International Atomic Energy Agency
LBE	Lead-Bismuth Eutectic
LES	Large Eddy Simulation
LFR	Lead-Cooled Fast Reactor
LMFR	Liquid Metal-cooled Fast Reactor
LWR	Light Water Reactor
MYRRHA	Multi-purpose hYbrid Research Reactor for High-tech Applications
NACIE	NAtural CIrculation Experiment
NC	Natural Circulation
O.D.	Outer Diameter
RANS	Reynold Averaged Navier Stokes
SEARCH	Safe ExploitAtion Related Chemistry for HLM reactors
SFR	Sodium-Cooled Fast Reactor
SYS-TH	System Thermal-hydraulic
TC	Thermocouple

Other Subscripts

A	Refers to section A
active	Refers to the active length
avg	Refers to average
B	Refers to section B
b	Refers to the bulk
C	Refers to section C
in	Refers to inlet
out	Refers to outlet
sc	Refers to the sub-channel
ss	Refers to the stainless steel
tot	Refers to the total bundle length
w	Refers to the wall

References

Abderrahim, H.A., Kupschus, P., Malambu, E., Benoit, Ph., Van Tichelen, K., Arien, B., Vermeersch, F., D'hondt, P., Jongen, Y., Ternier, S., Vandeplassche, D., 2001. MYRRHA: A multipurpose accelerator driven system for research & development, Nuclear Instruments and Methods in Physics Research A, 463, 487-494.

Alemberti, A., Smirnov, V., Smith, C.F., Takahashi, M., 2014. Overview of lead-cooled fast reactor activities, Progress in Nuclear Energy 77, 300-307.

Aoto K., Dufour P., Hongyi Y., Glatz J.P., Kim Y., Ashurko Y., Hill R., Uto N., 2014. A summary of sodium-cooled fast reactor development, Progress in Nuclear Energy 77, 247-265.

Bartholet, T. G., Roidt, R. M., Harper, L, J., 1977 a. Clinch River Breeder Reactor Plant 11:1 Scale Wire Wrapped Rod Bundle Air Flow Tests, Interior Subchannels, CRBRP-ARO-0108, January 1977. (Availability: U.S. DOE Technical Information Center).

Bartholet, T. G., Roidt, R. M., Romano, J, E., 1977 b. Clinch River Breeder Reactor Plant 11:1 Scale Wire Wrapped Rod Bundle Air Flow Tests, Side Subchannels, CRBRP-ARO-0108, January 1977. (Availability: U.S. DOE Technical Information Center).

Di Piazza, I., Tarantino, M., Agostini, P., Gaggini, P., Polazzi, G., Forgione, N., Martelli, D., 2013. NACIE-UP: an heavy liquid metal loop for mixed convection experiments with instrumented pin bundle, HLMC-2013, September 23-27, IPPE, Obninsk, Russian Federation.

Doolaard, H.J., Shams, A., Roelofs, F., Van Tichelen, K., Keijers, S., De Ridder, J., Degroote J., Vierendeels, Di Piazza, I., Marinari, R., Merzari, E., Obabko, A., Fischer P., 2015. CFD benchmark for a heavy liquid metal fuel assembly, Proc. NURETH-16, August 30- September 4, Chigaco, USA.

Fontana, M. H., Gnadt, P.A., MacPherson, R.E., Parsly, L.F., Wantland, J.L., 1973. Temperature distribution in a 19-rod simulated LMFBR fuel assembly in a hexagonal duct (fuel failure mockup bundle 2a) - record of experimental data, Technical Report ORNL-TM-4113, Oak Ridge National Laboratory.

Generation IV International Forum, 2014, January, Technology Roadmap Update for Generation IV Nuclear Energy Systems.

Gajapathy, R., Velusamy, K., Selvaraj, P., Chellapandi, P., Chetal, S.C., 2009. A comparative CFD investigation of helical wire-wrapped 7,19 and 37 fuel pin bundles and its extendibility to 217 pin bundle, Nucl. Eng. Des., 239, 2279-2292.

Khan, E.V., 1980. LMFBR In-Core Thermal-Hydraulics: The State of the Art and U. S. Research and Development Needs, Battelle Pacific Northwest Laboratory , PNL-3337/UC-32.

International Atomic Energy Agency (IAEA), 1999. LMFR core and heat exchanger thermohydraulic design: Former USSR and present Russian approaches, IAEA-tecdoc-1060, January 1999.

Lafay, J., Menant, B., Barroil, J., (1975). Local pressure measurements and peripheral flow visualization in a water 19-rod bundle compared with FLICA II B calculations: influence of helical wire-wrap spacer system, Proc. AICHE-ASME Heat Transfer Conf., Paper 75-HT-22, California, USA.

LeCharpentier, D., Thermocoax, private communication, 2015.

Le Coz, P., Sauvage, J.F.m, Serpantie, J.P., 2011. Sodium-cooled fast reactors the ASTRID plant project. Advances in Nuclear Power Plants International Congress proceedings. Nice, France, May 2–6.

Martelli, D., Forgione, N., Di Piazza, I., Tarantino, M., 2015. HLM fuel pin bundle experiments in the CIRCE pool facility, Nucl. Eng. Des. 292, 76-86.

Mikityuk, K., 2009. Heat transfer to liquid metal: Review of data and correlation for tube bundles, Nucl. Eng. Des. 239 (4), 680-687.

Nuclear Energy Agency, 2015. Handbook on Lead-bismuth Eutectic Alloy and Lead Properties, Materials Compatibility, Thermal-hydraulics and Technologies, OECD/NEA.

Pacio, J., Daubner, M., Fellmoser, F., Litfin, K., Marocco, L., Stieglitz, R., Taufall, S., Wetzel, Th., 2014. Heavy-liquid metal heat transfer experiment in a 19-rod bundle with grid spacer, Nucl. Eng. Des. 27, 33-46.

Pacio, J., Wetzel, Th., Doolaard, H.J., Roelofs, F., Van Tichelen, K., 2015. Thermal-hydraulic study of the LBE-cooled fuel assembly in the MYRRHA reactor: experiments and simulations, Proc. NURETH-16, August 30- September 4, Chigaco, USA.

Pfrang, W., Struwe, D., 2007. Assessment of Correlations for Heat Transfer to the Coolant for Heavy Liquid Metal Cooled Core Design, Technical Report FZKA 7352, Institut für Reaktorsicherheit, Karlsruhe.

Rolfo, S., Péniguel, C., Guillaud, M., Laurence, D., 2012. Thermal-hydraulic study of a wire spacer fuel assembly, Nucl. Eng. Des. 243, 251-262.

Tarantino, M., Martelli, D., Barone, G., Di Piazza, I., 2015. Mixed convection and stratification phenomena in a heavy liquid metal pool, Nucl. Eng. Des. 286, 261-277.

Turroni, P., Cinotti, L., Corsini, G., Mansani, L., 2001. The CIRCE facility, In: AccApp'01&ADTTA'01, Nuclear Application in the new Millennium, Reno, NV, USA, November 11–15.

Van Tichelen, K., SCK-CEN, private communication, 2015.

Wantland, J.L., Gnadt, P.A., MacPherson, R.E., Fontana, M.H., Hanus, N., , Smith, C.M., 1976. The effects of duct configuration on flow and temperature structure in sodium-cooled 19-rod simulated LMFBR fuel bundles with helical wire-wrap spacers, 16th National Heat Transfer Conference, St. Louis, MO, USA, 8-11 Aug 1976.